Azimuthal Drive Asymmetry in Inertial Confinement Fusion Implosions on the National Ignition Facility

Hans G. Rinderknecht*
Laboratory for Laser Energetics, University of Rochester, Rochester, New York 14623, USA

D. T. Casey, R. Hatarik, R. M. Bionta, B. J. MacGowan, P. Patel, O. L. Landen, E. P. Hartouni, and O. A. Hurricane
Lawrence Livermore National Laboratory, Livermore, California 94550, USA

(Received 20 December 2019; accepted 16 March 2020; published 10 April 2020)

Data from nuclear diagnostics present correlated signatures of azimuthal implosion asymmetry in recent indirect-drive inertial confinement fusion (ICF) implosion campaigns performed at the National Ignition Facility (NIF). The mean hot-spot velocity, inferred from the Doppler shift of 14 MeV neutrons produced by deuterium-tritium (DT) fusion, is systematically directed toward one azimuthal half of the NIF target chamber, centered on $\phi \approx 70°$. Areal density (ρR) asymmetry of the converged DT fuel, inferred from nuclear activation diagnostics, presents a minimum ρR in the same direction as the hot-spot velocity and with $\Delta\rho R$ amplitude correlated with velocity magnitude. These two correlated observations, which are seen in all recent campaigns with cryogenic layers of DT fuel, are a known signature of asymmetry in the fuel convergence, implying a systematic azimuthal drive asymmetry across a wide range of shot and target configurations. The direction of the implied radiation asymmetry is observed to cluster toward the hohlraum diagnostic windows. This low-mode asymmetry degrades hot-spot conditions at peak convergence and limits implosion performance and yield.

DOI: 10.1103/PhysRevLett.124.145002

Inertial confinement fusion (ICF) aims to ignite a propagating fusion burn wave in deuterium-tritium (DT) fuel. Ignition requires fuel self-heating by fusion-produced alpha particles to exceed losses due to expansion, thermal conduction, and radiative cooling. Calculating these terms produces an ignition condition (the "Lawson criterion" [1]), which is often cast as a lower limit on the product of the hot-spot pressure P and confinement time τ: $P\tau \gtrsim 10$ atm sec [2]. In hot-spot ignition ICF, short (~100 ps) confinement time is exchanged for high (>300 Gbar) hot-spot pressures, which are produced by spherical implosion of a cryogenic fuel layer with a ratio of initial to final radius in excess of 30 [3]. The currently best-performing ICF implosions on the National Ignition Facility (NIF) have produced hot-spot pressures of 360 Gbar and fusion yields of 50 kJ and have begun to show the effects of fusion self-heating [4]. However, these experiments continue to underperform simulations of their performance, which predict pressures above 500 Gbar and dynamics dominated by self-heating.

The large radial convergence required for hot-spot ignition places demanding requirements on the symmetry of the implosion. Asymmetric convergence produces unstagnated flows in the converged fuel and hot spot, which limits the maximum hot-spot pressure and reduces confinement time [5]. Much of the effort in the NIF implosion campaigns focuses on controlling hot spot asymmetries, which are diagnosed using time-dependent x-ray self-emission imaging and neutron hot-spot imaging [6]. These diagnostics generally lack, however, an absolute position reference and are therefore not sensitive to offsets in the implosion, described by the first spherical harmonic or "mode-1" asymmetry. Simulations have shown that an offset drive illuminating one side of a capsule more brightly than the opposite can produce a net velocity in the fusing hot spot and significant asymmetry in fuel assembly [7]. Such flows have been measured using time-resolved x-ray pinhole cameras [8], but the accuracy of this technique is limited by the small number of diagnostic views. Asymmetry in the assembled fuel has been suggested by trends in hot-spot areal density, ion temperature, and pressure [9], and from significant variations of scattered neutron flux with line-of-sight observed on some implosions [10].

This Letter presents experimental evidence from nuclear diagnostics of a systematic mode-1 drive asymmetry in the cryogenic implosion campaigns on the NIF. Flows in the hot-spot plasma are diagnosed by measuring the Doppler shift of the fusion neutrons: these flows are often a significant fraction of the implosion velocity and systematically concentrate toward one direction perpendicular to the axis of hohlraum symmetry. The local areal density (ρR) of the converged fuel is diagnosed by variations in the neutron fluence as measured by neutron activation

diagnostics (NADs): the asymmetry magnitude correlates strongly with velocity magnitude, and the direction of minimum ρR matches the direction of hot-spot velocity. These observations together strongly indicate the presence of an unexpected systematic implosion asymmetry in NIF cryogenic implosions over the past three years. Such an asymmetry limits the performance of the present ICF implosions and must be corrected if ignition is to be achieved.

The converged hot spot produces neutrons via two reactions: deuterium-tritium (DT) and deuterium-deuterium (DD) fusion. These reactions produce neutrons with birth energies of 14.02 and 2.45 MeV, respectively; however, the spectral shape is modified by both local temperature and velocity [11]. Neutron time-of-flight (nTOF) spectrometers view the implosion from four positions around the NIF target chamber [12]. Since these spectrometers record neutrons produced throughout the fusing volume, the spectral shape can be fit to infer the "burn-weighted" hot-spot conditions. In particular, a neutron-averaged flow velocity projected along each detector line of sight is obtained by observing the shift in mean neutron energy relative to the expected value [13]. Using at least three of these measurements, the mean hot-spot velocity magnitude and direction can be determined, along with rigorous uncertainty estimates [14]. (Directions are in NIF polar coordinates θ, ϕ that are angles relative to the hohlraum axis and azimuth, respectively.)

Applying this method to 44 implosions with cryogenic DT-ice layers performed on the NIF during 2016–2018, a pattern emerges, as shown in Fig. 1. For implosions in which significant velocity was inferred ($V > 30$ km/s, a typical value for the measurement uncertainty), the hot spots are observed to flow toward one hemisphere. This dataset includes experiments that use a variety of laser pulse shapes and ablators, including shots from the high-density carbon (HDC) [15], "Bigfoot" (high-adiabat HDC) [16], and CH campaigns [17]. The three campaigns are not equally susceptible to the azimuthal velocity asymmetry. Significant velocities were observed in 17 of 18 HDC and 10 of 11 Bigfoot implosions, including one shot in each campaign exceeding 115 km/s. In contrast, only 6 of 15 CH implosions in the data set had significant velocity, with a maximum of 90 km/s. However, the clustering of hot-spot flow direction toward one-half of NIF azimuthal space (approximately $-20° < \phi < 160°$) was observed in all three campaigns. The implosions used hohlraums with diagnostic windows (regions of the hohlraum wall with thinner gold layers) toward $\phi = 79°$ and 100° ("2-window"), and with an additional window toward $\phi = 315°$ ("3-window"). The 2-window hohlraums are observed to produce hot-spot velocities on average in the direction $\phi = 94° \pm 35°$, whereas 3-window hohlraums produce velocities toward $\phi = 63° \pm 57°$: consistent with the average of the window directions in each design. This systematic difference suggests the windows contribute to the

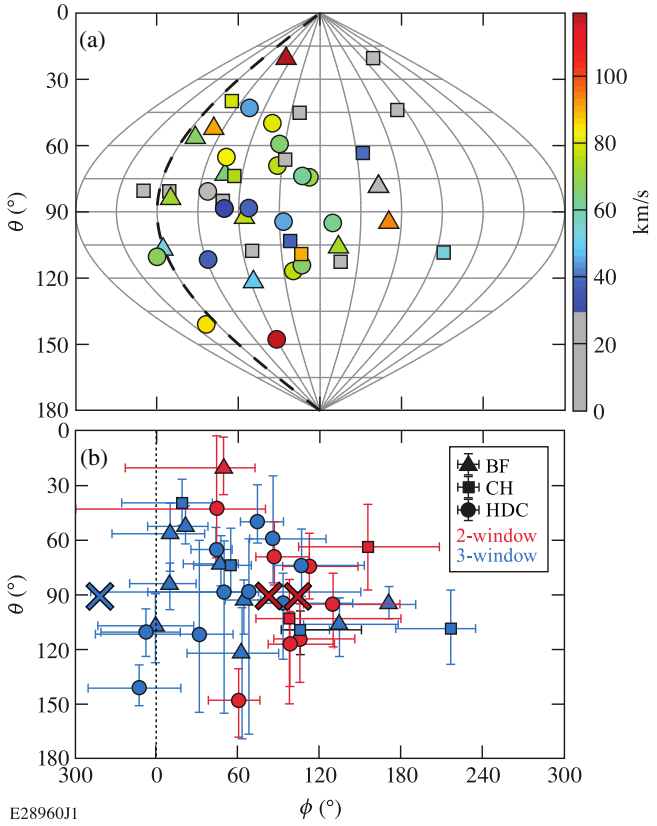

FIG. 1. (a) Neutron-averaged hot-spot flow velocity magnitude and direction evaluated for NIF cryogenic implosions in the HDC (Circle), Bigfoot (Triangle), and CH (Square) campaigns from 2016–2018. The gray symbols represent implosions with bulk velocity below 30 km/s. (b) Uncertainty in the inferred hot-spot velocity direction for implosions with $V > 30$ km/s. Color indicates hohlraum designs with 2 (red) or 3 (blue) diagnostic windows with positions indicated by the × signs.

observed trend. It is worth noting the magnitude of the velocities observed: many of the implosions presented velocities in excess of 20% of the implosion velocity (typically 350 to 420 km/s). The observed hot-spot velocities represent significant perturbations to the implosions' uniformity.

As neutrons leave the hot spot, they have a chance of scattering in the converged DT-fuel layer, which is comparatively cold ($T \sim 0.5$ keV) and dense ($\rho \sim 100$ g/cm^3). This scattering process provides a means of diagnosing the ρR of the converged fuel at the time of peak neutron production. The probability of a primary DT-fusion neutron transiting the fuel is

$$P = \exp\left[-\frac{\rho R \sigma_{(n,\mathrm{DT})}}{M_{\mathrm{DT}}}\right], \tag{1}$$

where $\sigma_{(n,\mathrm{DT})} = f_{\mathrm{D}}\sigma_{(n,\mathrm{D})} + f_{\mathrm{T}}\sigma_{(n,\mathrm{T})}$ is the mean cross section for neutron scattering, $M_{\mathrm{DT}} = f_{\mathrm{D}}M_{\mathrm{D}} + f_{\mathrm{T}}M_{\mathrm{T}}$ is the mean atomic mass of the fuel, and f_{D}, f_{T} are the

concentration fractions of deuterium and tritium, respectively. For equimolar D:T mixtures ($f_D = f_T = 0.5$), the average cross section is approximately 0.79 b and the probability of scattering is $(1 - P) \approx 0.19 \times \rho R/(\mathrm{g/cm^2})$.

On the NIF, a suite of neutron activation diagnostics is used to infer the fluence of unscattered neutrons on over 20 lines of sight [18]. This measurement records the activation of zirconium-90 atoms via the $^{90}\mathrm{Zr}(n, 2n)^{89}\mathrm{Zr}$ reaction, which has a neutron energy threshold of 12 MeV and a cross section that increases roughly linearly in the range 12 to 16 MeV [19]. Scattered neutrons lose energy, reducing or eliminating the probability of $^{90}\mathrm{Zr}$ activation. Because of this, variations in ρR are encoded as inverse perturbations in the map of detector activation. The sensitivity of the activation cross section to neutron energy makes this measurement also susceptible to the effects of hot-spot velocity, directly via the Doppler shift and kinematic focusing and indirectly via small changes in the scattering cross sections. However, the independent measurement of the hot-spot velocity from the nTOF diagnostics enables one to correct the activation detectors for these velocity effects and recover the variation due to scattering [14]. If scattered neutrons are assumed to be lost from detection, the variation in areal density ($\Delta\rho R$) can be calculated from the variation in activation A relative to the mean value $\langle A \rangle$ as

$$\Delta\rho R \approx -\frac{M_{\mathrm{DT}}}{\sigma_{(n,\mathrm{DT})}} \ln\left[\frac{A}{\langle A\rangle}\right] \sim -\ln\left[\frac{A}{\langle A\rangle}\right] 4.64\ \mathrm{g/cm^2}. \quad (2)$$

Figure 2(a) shows a representative activation map from shot N180909 (Bigfoot series, producing 1.2×10^{16} DT neutrons). After correcting for an observed hot-spot velocity of 94 km/s in the direction $(\theta, \phi) = (95^{\circ+8}_{-9}, 171^{\circ+20}_{-26})$, the residual activation data showed variations in the range $\pm 9\%$. (The velocity correction accounted for approximately 30% of the asymmetry in the raw activation data, typical for this dataset.) A fit of first- and second-mode spherical harmonics to the data demonstrated that the dominant asymmetry was a mode-1 asymmetry with an amplitude of $4.1\% \pm 0.8\%$ in the direction $(87^{\circ+13}_{-9}, 142^{\circ+26}_{-19})$ [20]. Using Eq. (2), this mode corresponds to an areal density asymmetry of ∓ 0.19 g/cm^2: one-third of the average fuel ρR inferred from other diagnostics (0.59 g/cm^2).

Performing the activation analysis for the 2016–2018 NIF cryogenic experiments produces a similar pattern to that observed in the velocity data. Figure 2(b) shows the magnitudes and directions of the mode-1 asymmetries inferred from the activation data, for shots with magnitude greater than 2.5%. This set includes 12 of 18 HDC, 9 of 11 Bigfoot, and 7 of 15 CH implosions, comparable to the number of implosions that presented significant hot-spot velocities. The data again cluster by hohlraum window

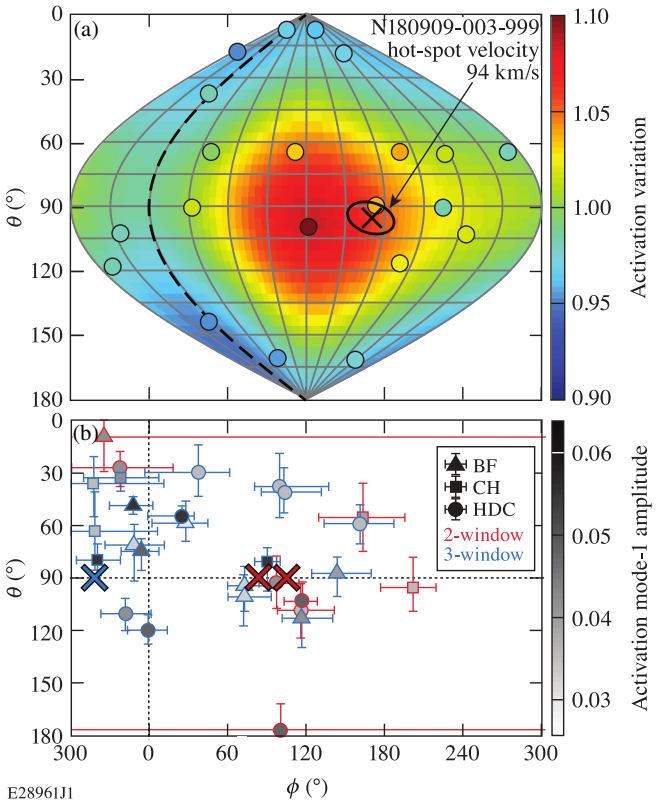

FIG. 2. (a) Activation data (points) and best-fit map for Bigfoot shot N180909. Data have been corrected for an inferred hot-spot velocity (black × with uncertainty boundary). A dominant mode-1 asymmetry is observed in the activation signal. (b) Uncertainty in the inferred direction of mode-1 asymmetry for implosions with mode-1 asymmetry above 2.5%. The amplitude of the mode-1 asymmetry for each shot is shown in gray scale.

design toward the same regions of azimuthal space as is observed in the velocity data.

Figure 3 presents a more thorough comparison between the magnitudes and directions of the hot-spot velocity and activation asymmetry measurements. The inferred areal density asymmetry [from Eq. (2)] normalized to the average areal density is plotted in Fig. 3(a).The magnitudes of the two signatures are observed to scale linearly across the entire dataset: a best-fit slope of 39% ρR mode-1 asymmetry per 100 km/s hot-spot velocity matches the data with a reduced χ^2 metric of 0.3. The hypothesis that the (θ, ϕ) directions of the hot-spot velocity and activation mode-1 are the same is supported with reduced χ^2 values of 0.7 and 0.6, respectively. These low values of the reduced χ^2 metric suggest that the measurement uncertainties are likely overestimated. The comparison of the azimuthal angle in Fig. 3(c) clearly shows the clustering of data points into the range $-20^{\circ} \lesssim \phi \lesssim 160^{\circ}$, and the denser clustering of 2-window shots toward $\phi \approx 90^{\circ}$ in both diagnostics.

The striking coincidence of magnitude and direction in these two independent nuclear diagnostic signatures across

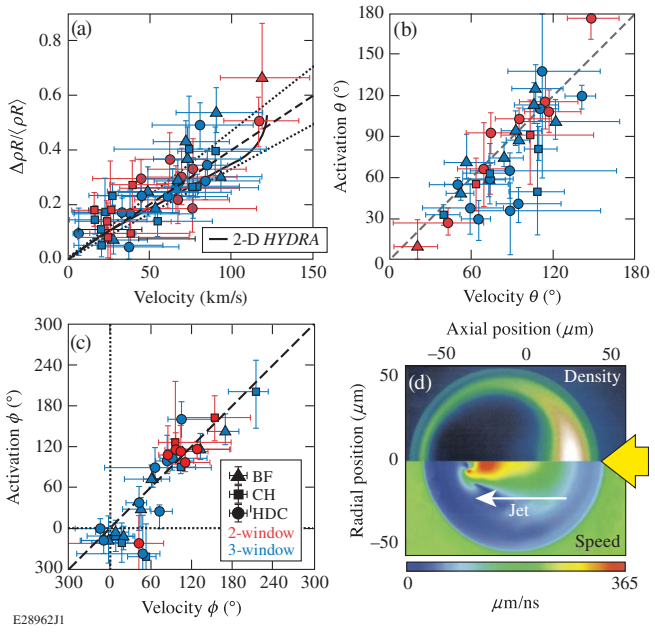

FIG. 3. Comparisons of ρR mode-1 asymmetry and hot-spot velocity (a) magnitude and (b),(c) direction. The normalized ρR mode-1 amplitudes increase linearly with hot-spot velocity with a slope of 39%±7% per 100 km/s (gray dashed), consistent with the trend predicted in 2D simulations of a mode-1 drive asymmetry (black) [7]. Directions are plotted for shots with velocity in excess of 30 km/s, and ϕ uncertainty below 270°. The θ and ϕ directions of the two signatures are consistent, and both velocity and mode-1 amplitude cluster in the azimuthal range $-20° \lesssim \phi \lesssim 160°$. (d) Two-dimensional simulations of density and velocity profiles at peak neutron production with 2% mode-1 drive asymmetry [21].

a wide range of experiments with varied designs (ablator composition, target dimensions, laser energy, time history, etc.) performed over a period of three years suggests a common, systematic underlying cause. Asymmetry in the capsule drive is the most straightforward explanation for these coordinated signatures. Spears *et al.* [7] performed 2D simulations of radiation-driven implosions with an imposed mode-1 asymmetry in the radiation intensity. While this work was motivated by the possibility of pole-to-pole asymmetry, the result does not consider hohlraum geometry and is generally applicable to radiation asymmetry in arbitrary directions. The simulated drive asymmetry produced a net ablation pressure imbalance, accelerating the capsule away from the direction with higher radiation flux. In these simulations, the neutron-weighted hot-spot velocity was directed away from the peak intensity, increased with drive asymmetry up to 2% peak-to-mean intensity, and covered the range of magnitudes observed in this work (≤ 120 km/s). Areal density also increased in the direction of peak intensity and decreased in the opposite direction. Simulated activation detectors observed mode-1 asymmetry directed away from the peak intensity and reaching 8% (after velocity correction) at 2% drive asymmetry. From these simulated results, a prediction of the scaling between neutron-inferred hot-spot velocity and areal density asymmetry magnitude was determined, as shown in Fig. 3(a). The data are consistent with the simulated trend (approximately 38% per 100 km/s).

The hohlraum windows can plausibly create such a mode-1 radiation asymmetry. Figure 4 shows a calculation of the reduction in radiation flux onto a capsule inside a 3-window hohlraum, assuming complete radiation loss at the windows, performed using the view factor code VisRAD [22]. Up to 6.2% radiation deficit toward the windows is predicted in this limiting case: significantly larger than the asymmetry needed to explain the most extreme velocities. In experiments, thinner gold layers and gaps approaching half the window area will reduce local radiation power by some fraction of this amount, inducing velocity and higher activation in the average direction of the windows. This hypothesis matches the observed data trends with hohlraum window design. Together, these observations provide strong evidence that a systematic, azimuthally directed mode-1 drive asymmetry of up to ±2% in radiation intensity is present in this series of implosions. Detailed models are in development to more quantitatively assess window radiation losses, including the effects of window architecture and ablation dynamics [23,24].

Several recent works have investigated the effects of asymmetry on implosion performance in both direct-drive [25,26] and indirect-drive ICF [5,7,27]. The work by Springer *et al.* [5] applies a simplified 3D fuel convergence model to the HDC shot N170601, which is included in the dataset considered here. This shot produced a neutron-inferred hot-spot velocity of 66 ± 39 km/s toward ($59°^{+24}_{-35}$, $85°^{+39}_{-17}$) and a velocity-corrected amplitude asymmetry of $3.5\% \pm 1.0\%$ toward ($38°^{+18}_{-19}$, $99°^{+38}_{-19}$). The model found that a 1% initial shape error at an imploding radius of 200 μm was sufficient to match the observed activation

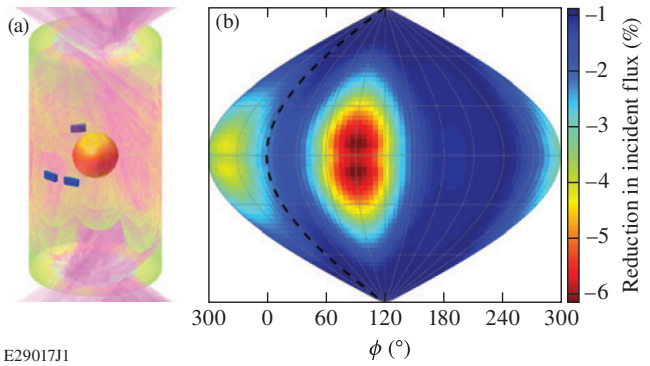

FIG. 4. (a) Model of the capsule in a laser-irradiated hohlraum from view angle (65°, 120°). Size and position of diagnostic windows are shown in blue. (b) Calculated reduction of radiation flux on the capsule in a 3-window hohlraum, assuming complete radiation loss through the windows.

mode-1 and mode-2 asymmetries. This perturbation degraded the nuclear yield by 5× and the stagnation pressure by 20%. While additional degradation mechanisms were needed to match the experimental performance, the low-mode implosion asymmetry represented the single largest degradation mechanism of those considered [5].

On the basis of these data a research program has been initiated to find and control the origins of the drive asymmetry, which remains a crucial step for ongoing efforts to achieve ignition on the NIF. The data imply that the hohlraum radiation drive is systematically weaker toward $\phi \sim 70°$. Preliminary results indicate that the sources of this mode-1 drive asymmetry include the hohlraum windows and laser delivery, each contributing on the order of 0.5% [23,28]. Additional smaller contributions are anticipated from capsule thickness variations, ice layer thickness variations, and laser-to-target misalignment. The capsule fill tube ($\phi \sim 7°$) [29] is not likely to be a significant contributor. The magnitudes and mitigations for these factors are the subject of ongoing review, and the results of this active research program will be discussed in forthcoming works. Improved diagnostics, including more accurate Cherenkov neutron spectrometers [30] and an expanded set of 48 activation detectors [31] will reduce uncertainty in the observed signatures of asymmetry. Including additional diagnostics in this analysis, such as reconstructions of the cold fuel from down-scattered neutron images [32], will also improve the understanding of these asymmetries and constraints on probable causes.

In summary, two nuclear diagnostic signatures of azimuthal implosion asymmetry have been observed in indirect-drive cryogenic implosion experiments on the NIF in the period 2016–2018. Neutron-weighted hot-spot velocity is observed to be clustered toward one-half of NIF azimuthal space centered on $\phi \sim 70°$, often above 15% of the implosion velocity. The nuclear activation diagnostics report mode-1 asymmetries that indicate low areal density in the same direction as the hot-spot velocity, and the magnitude of these two phenomena scale linearly. These observations are signatures of a systematic, azimuthal mode-1 drive asymmetry in the NIF hohlraum, with the weakest drive intensity on average in the direction of the hohlraum windows. Work to identify and control the source of this asymmetry is ongoing and will be essential to further improving implosion performance and achieving ignition in indirect-drive ICF.

This material is based upon work supported by the Department of Energy National Nuclear Security Administration under Award No. DE-NA0003856, the University of Rochester, and the New York State Energy Research and Development Authority. This report was prepared as an account of work sponsored by an agency of the U.S. Government. Neither the U.S. Government nor any agency thereof, nor any of their employees, makes any warranty, express or implied, or assumes any legal liability or responsibility for the accuracy, completeness, or usefulness of any information, apparatus, product, or process disclosed, or represents that its use would not infringe privately owned rights. Reference herein to any specific commercial product, process, or service by trade name, trademark, manufacturer, or otherwise does not necessarily constitute or imply its endorsement, recommendation, or favoring by the U.S. Government or any agency thereof. The views and opinions of authors expressed herein do not necessarily state or reflect those of the U.S. Government or any agency thereof.

*hrin@lle.rochester.edu

[1] J. D. Lawson, Proc. Phys. Soc. London Sect. B **70**, 6 (1957).
[2] R. Betti, P. Y. Chang, B. K. Spears, K. S. Anderson, J. Edwards, M. Fatenejad, J. D. Lindl, R. L. McCrory, R. Nora, and D. Shvarts, Phys. Plasmas **17**, 058102 (2010).
[3] S. W. Haan, J. D. Lindl, D. A. Callahan, D. S. Clark, J. D. Salmonson, B. A. Hammel, L. J. Atherton, R. C. Cook, M. J. Edwards, S. Glenzer *et al.*, Phys. Plasmas **18**, 051001 (2011).
[4] S. Le Pape, L. F. Berzak Hopkins, L. Divol, A. Pak, E. L. Dewald, S. Bhandarkar, L. R. Bennedetti, T. Bunn, J. Biener, J. Crippen *et al.*, Phys. Rev. Lett. **120**, 245003 (2018).
[5] P. Springer, O. Hurricane, J. Hammer, R. Betti, D. Callahan, E. Campbell, D. Casey, C. Cerjan, D. Cao, E. Dewald *et al.*, Nucl. Fusion **59**, 032009 (2019).
[6] M. J. Edwards and Ignition Team, J. Phys. Conf. Ser. **688**, 012017 (2016).
[7] B. K. Spears, M. J. Edwards, S. Hatchett, J. Kilkenny, J. Knauer, A. Kritcher, J. Lindl, D. Munro, P. Patel, H. F. Robey *et al.*, Phys. Plasmas **21**, 042702 (2014).
[8] J. J. Ruby, A. Pak, J. E. Field, T. Ma, B. K. Spears, L. R. Benedetti, D. K. Bradley, L. F. Berzak Hopkins, D. T. Casey, T. Döppner *et al.*, Phys. Plasmas **23**, 072701 (2016).
[9] O. A. Hurricane, D. A. Callahan, D. T. Casey, E. L. Dewald, T. R. Dittrich, T. Dppner, S. Haan, D. E. Hinkel, L. F. Berzak Hopkins, O. Jones *et al.*, Nat. Phys. **12**, 800 (2016).
[10] C. B. Yeamans and N. Gharibyan, Rev. Sci. Instrum. **87**, 11D702 (2016).
[11] D. H. Munro, Nucl. Fusion **56**, 036001 (2016).
[12] T. J. Clancy, J. Caggiano, J. McNaney, M. Eckart, M. Moran, V. Y. Glebov, J. Knauer, R. Hatarik, S. Friedrich, R. Zacharias *et al.*, Proc. SPIE Int. Soc. Opt. Eng. **9211**, 92110A (2014).
[13] R. Hatarik, R. C. Nora, B. K. Spears, M. J. Eckart, G. P. Grim, E. P. Hartouni, A. S. Moore, and D. J. Schlossberg, Rev. Sci. Instrum. **89**, 10I138 (2018).
[14] H. G. Rinderknecht, R. Bionta, G. Grim, R. Hatarik, H. Khater, D. Schlossberg, and C. Yeamans, Rev. Sci. Instrum. **89**, 10I125 (2018).
[15] L. B. Hopkins, S. LePape, L. Divol, A. Pak, E. Dewald, D. D. Ho, N. Meezan, S. Bhandarkar, L. R. Benedetti, T. Bunn *et al.*, Plasma Phys. Controlled Fusion **61**, 014023 (2019).
[16] D. T. Casey, C. A. Thomas, K. L. Baker, B. K. Spears, M. Hohenberger, S. F. Khan, R. C. Nora, C. R. Weber,

D. T. Woods, O. A. Hurricane *et al.*, Phys. Plasmas **25**, 056308 (2018).
[17] O. A. Hurricane, P. T. Springer, P. K. Patel, D. A. Callahan, K. Baker, D. T. Casey, L. Divol, T. Dppner, D. E. Hinkel, M. Hohenberger *et al.*, Phys. Plasmas **26**, 052704 (2019).
[18] C. B. Yeamans and D. L. Bleuel, Fusion Sci. Technol. **72**, 120 (2017).
[19] M. B. Chadwick, P. Obložinský, M. Herman, N. M. Greene, R. D. McKnight, D. L. Smith, P. G. Young, R. E. MacFarlane, G. M. Hale, S. C. Frankle *et al.*, Nucl. Data Sheets **107**, 2931 (2006).
[20] The quoted uncertainty in the amplitude includes both the statistical uncertainty of the activation detectors $(A, \theta, \phi) \sim (0.49\%, 5°, 7°)$ and the propagated uncertainty due to velocity correction $\sim(0.63\%, 10°, 22°)$.
[21] Fig. 3(d) reprinted from B. K. Spears *et al.*, Phys. Plasmas **21**, 042702 (2014), with the permission of AIP Publishing.
[22] J. J. MacFarlane, J. Quant. Spectrosc. Radiat. Transfer **81**, 287 (2003).
[23] B. J. MacGowan, O. L. Landen, D. A. Callahan, D. T. Casey, E. P. Hartouni, R. Hatarik, M. Hohenberger, T. Ma, D. Mariscal, A. Moore *et al.*, High Energy Dens. Phys. (to be published).
[24] J. Milovich, D. T. Casey, O. Jones, and O. Landen, Bull. Am. Phys. Soc. **64**, JO7.00005 (2019), http://meetings.aps.org/Meeting/DPP19/Session/JO7.5.
[25] A. Bose, R. Betti, D. Shvarts, and K. M. Woo, Phys. Plasmas **24**, 102704 (2017).
[26] A. Bose, R. Betti, D. Mangino, K. M. Woo, D. Patel, A. R. Christopherson, V. Gopalaswamy, O. M. Mannion, S. P. Regan, V. N. Goncharov *et al.*, Phys. Plasmas **25**, 062701 (2018).
[27] B. Cheng, T. J. T. Kwan, S. A. Yi, O. L. Landen, Y. M. Wang, C. J. Cerjan, S. H. Batha, and F. J. Wysocki, Phys. Rev. E **98**, 023203 (2018).
[28] B. J. MacGowan, O. Landen, D. Casey, C. Young, P. Michel, D. Callahan, J.-M. Di Nicola, D. Mariscal, T. Ma, J. Milovich *et al.*, Bull. Am. Phys. Soc. **64**, JO7.00010 (2019), http://meetings.aps.org/Meeting/DPP19/Session/JO7.10.
[29] D. S. Clark, C. R. Weber, J. L. Milovich, A. E. Pak, D. T. Casey, B. A. Hammel, D. D. Ho, O. S. Jones, J. M. Koning, A. L. Kritcher *et al.*, Phys. Plasmas **26**, 050601 (2019).
[30] D. J. Schlossberg, A. S. Moore, B. V. Beeman, M. J. Eckart, G. P. Grim, E. P. Hartouni, R. Hatarik, M. S. Rubery, D. B. Sayre, and C. Waltz, Rev. Sci. Instrum. **89**, 10I136 (2018).
[31] J. R. Root, D. R. Jedlovec, E. R. Edwards, C. B. Yeamans, T. Golod, J. Hernandez, P. Adams, and G. Brunton, Proc. SPIE Int. Soc. Opt. Eng. **10390**, 103900J (2017).
[32] D. T. Casey, P. L. Volegov, F. E. Merrill, D. H. Munro, G. P. Grim, O. L. Landen, B. K. Spears, D. N. Fittinghoff, J. E. Field, and V. A. Smalyuk, Rev. Sci. Instrum. **87**, 11E715 (2016).